Generalized Stability of Nongeostrophic Baroclinic Shear Flow. Part I: Large Richardson Number Regime

EYAL HEIFETZ

Department of Geophysics and Planetary Sciences, Tel-Aviv University, Tel Aviv, Israel

BRIAN F. FARRELL

Division of Applied Sciences, Harvard University, Cambridge, Massachusetts

(Manuscript received 6 November 2000, in final form 14 January 2003)

ABSTRACT

A generalized stability theory (GST) analysis of baroclinic shear flow is performed using primitive equations (PEs), and typical synoptic-scale midlatitudinal values of vertical shear and stratification. GST is a comprehensive linear stability theory that subsumes modal stability theory and extends it to account for nonmodal interactions such as may occur among the approximately geostrophically balanced modes and the nearly divergent gravity wave modes supported by the PE. Unbounded constant shear flow and the Eady model are taken as examples and energy is used as the reference norm. Comparison is made with results obtained using quasigeostrophic (QG) analysis. While the PE and the QG dynamics give similar results for timescales of a few days, the PE initial growth rate during the first few hours exceeds the QG growth at all wavelengths and can attain values as much as two orders of magnitude greater as the wavelength decreases. This PE growth is due both to the direct kinetic energy growth mechanism, which is filtered out by QG, and to the interaction between the QG modes and the gravity waves.

An important application of GST is to study shear turbulence using a method of analysis based on stochastically forcing the mean state. The PE response of the Eady model to spatially and temporally uncorrelated forcing reveals the rotational and the divergent modes support a comparable amount of variance. The observed spectrum and physical mechanisms influencing the spectrum are discussed.

1. Introduction

Quasigeostrophy (QG) provides a theoretical basis for understanding atmospheric dynamics at the synoptic scale including the essential nature of cyclone development. However, QG theory is strictly valid only in the limit of a small Rossby number and a large Richardson number (flows strongly constrained by rotation and stratification), and in the midlatitude atmosphere, these constraints are often quantitatively violated, particularly in association with strong cyclogenesis and frontogenesis. In order to secure and extend understanding of synoptic-scale dynamics, the effects of relaxing the QG assumptions must be determined. A necessary first step in exploring the effects of relaxing the QG constraints is to examine nongeostrophic dynamics in the linear limit. This problem has been studied previously using the method of modal analysis (e.g., Áranson 1963; Stone 1966; Derome and Dolph 1970; Mankin 1977; Bannon 1989; Nakamura 1988; Snyder 1995; Yamazaki and Peltier 2001) but because atmospheric flows are generally highly nonnormal, a comprehensive assessment of linear stability of these flows requires the methods of generalized stability theory (GST; Farrell and Ioannou 1996, hereafter FI96) used in this study. GST subsumes modal stability theory and extends it to comprehensively account for all growth processes by including the interaction among modes and the mean flow regardless of whether the modes are unstable or not. This comprehensiveness is crucial to understanding interactions between the approximately balanced geostrophic modes and the approximately divergent gravity wave modes that lie at the center of the concept of isolating a rotationally balanced slow manifold. We find that modal interaction increases strongly with the mean shear so that orthogonality between the approximately balanced and divergent manifolds on which this concept is based is lost as shear increases.

GST advances the study of nongeostrophic dynamics in another crucial way by allowing approximate solution for the fully turbulent state by analysis of the stochastically forced mean shear (FI96). Such an extension of stability theory to analyze the turbulent state is not possible using the method of modes. In the present case of

Corresponding author address: Eyal Heifetz, Dept. of Geophysics and Planetary Sciences, Tel-Aviv University, 69978 Tel Aviv, Israel. E-mail: eyalh@cyclone.tau.ac.il

the primitive equation (PE) it allows solution for the complete spectrum of waves so that physical mechanisms maintaining the equilibrium spectra can be examined in detail separating the turbulent forcing from the linear shear growth and dissipation processes.

Among the effects of nongeostrophic dynamics in the presence of baroclinic shear are modification of the primarily rotationally constrained Rossby waves, which are supported in QG and, in addition, the excitation and growth of new waves with primarily ageostrophic balance, which are not supported in QG. Moreover, separation of these wave manifolds is not absolute except in the limit of vanishing shear, and the interaction between primarily rotational and primarily divergent waves in the presence of shear is a central issue in nongeostrophic dynamics (Blumen 1975; Warn and Menard 1986; Dewar and Killworth 1995). A related issue is the nature of geostrophic adjustment in the presence of strong shear where the conceptual separation of gravity waves and Rossby waves as independent agents in the adjustment process, which was so useful in the unsheared case, can no longer be justified. As we shall see, even for small shear this interaction can produce very large growth rates over short times. Understanding the process by which the primarily divergent velocity field of the gravity wave in the presence of small shear is able to advect the primarily geostrophic thermal field to produce a short time perturbation growth is at least useful for interpreting results of short time adjoint optimizations and short time singular vectors associated with variational data assimilation and ensemble generation algorithms used in forecast models.

These issues of orthogonality among modes relate to understanding the observed confinement of synoptic- and subsynoptic-scale disturbances in midlatitudes to a primarily geostrophic balance. Among the explanations that have been advanced for this phenomenon are that the potential for disturbance growth is confined to the primarily rotational modes and that rapid adjustment continually returns disturbances with divergent components back to the primarily rotational manifold. We examine these mechanisms below and find that the potential growth of ageostrophic disturbances in fact exceeds that of primarily geostrophic disturbances and that the primarily nongeostrophic modes are also highly persistent. We conclude that the observed approximately rotationally balanced state occurs in part because the essentially stochastic forcing arising from the turbulence is correlated in time, and that the divergent motions are subject to enhanced dissipation compared to rotational modes at the same scale. Applied to shear flows, this stochastic turbulence model allows a separation between, on the one hand, nonlinear mechanisms and other processes that enter as the forcing, and on the other, the amplification process, which is solved for explicitly using the linear dynamics. In QG the forcing can be adequately modeled as white in space and time (FI95), which is a welcome simplification, but in this work we find that the higher frequencies of the gravity waves require taking account of the temporal correlation of the forcing.

We choose the Eady problem as an example to examine nongeostrophic dynamics because of its simplicity and because there are a number of previous works based on this model, so the properties of this model are familiar (Stone 1966; Farrell 1984; Nakamura 1988; Bannon 1989; Yamazaki and Peltier 2001). In this paper (Part I) we analyze the generalized stability properties of nongeostrophic synoptic-scale dynamics for typical midlatitude values of mean baroclinic shear $\Lambda = \overline{U}_z = O(10^{-3}\ \mathrm{s}^{-1})$ and stratification $N = O(10^{-2}\ \mathrm{s}^{-1})$ corresponding to Richardson number $\mathrm{Ri} = (N/\Lambda)^2 = O(100)$. The baroclinic PEs are introduced in section 2 and a 3D Helmholtz decomposition-based formulation for solving the PE is described. The Eady model is reviewed and its optimal growth explored as a function of spatial scale in section 3. The response of the system to stochastic forcing is examined in section 4, and we conclude with a discussion of our results in section 5.

In a forthcoming companion paper (hereafter Part II) the generalized stability of nongeostrophic dynamics for intermediate and small Richardson numbers is examined. A small Richardson number corresponds to a combination of larger shear and smaller static stability than is typical for midlatitude synoptic-scale motions but for which a strong interaction occurs between the approximately balanced modes and the gravity waves.

2. Formulation

a. The baroclinic primitive equations in unbounded shear

The momentum, thermodynamic and continuity equations linearized about a basic-state zonal wind with constant vertical shear $\overline{U} = \Lambda z$ are

$$\frac{du}{dt} = fv_a - \Lambda w, \tag{1a}$$

$$\frac{dv}{dt} = -fu_a, \tag{1b}$$

$$\frac{dw}{dt} = -\phi_z + \theta \tag{1c}$$

$$\frac{d\theta}{dt} = f\Lambda v - N^2 w, \tag{1d}$$

$$u_{ax} + v_{ay} + w_z = 0. \tag{1e}$$

In (1) the linearized substantial derivative is denoted by $d/dt \equiv \partial/\partial t + \overline{U}(\partial/\partial x)$; the Boussinesq approximation is made, and a constant value of the Coriolis parameter f and a constant mean stratification are assumed so that $N^2 = (g/\theta_0)\overline{\theta}_z$, where N is the Brunt–Väisälä frequency. The mean zonal shear is assumed to be in thermal wind balance $f\Lambda = -(g/\theta_0)\overline{\theta}_y$, where $\overline{\theta}/\theta_0$ is the mean state

potential temperature scaled by a representative tropospheric value and g is the constant gravitational acceleration. The zonal, meridional, and vertical directions are denoted (x, y, z) respectively, and the total vector velocity perturbation is $\mathbf{u} = (u, v, w) = \mathbf{u}_g + \mathbf{u}_a$, where $\mathbf{u}_g = (u_g, v_g, 0)$ and $\mathbf{u}_a = (u_a, v_a, w_a)$ are the geostrophic and ageostrophic components. The geostrophic component of the perturbation velocity is $\mathbf{u}_g = f^{-1}(-\phi_y, \phi_x, 0)$, where ϕ is the geopotential perturbation in log pressure coordinates.

The QG equations differ from (1) in assuming that the substantial derivative of the horizontal velocity components on the lhs of (1a) and (1b) involves only the geostrophic components of the velocity by assuming quasi-hydrostatic balance [vanishing of the lhs of (1c)] and by neglecting the advection of the mean wind by the vertical component of perturbation velocity [the term Λw on the rhs of (1a)]. As a result of the latter, the QG framework excludes the mechanism of energy transfer from the mean to the perturbation mediated by Reynolds stress.

b. An upper bound on energy growth

In the QG limit, the growth of volume-integrated total perturbation energy can be shown to be (e.g., Gill 1982, p. 566)

$$\frac{\partial}{\partial t}\int E_{qg}\,dV = \frac{\partial}{\partial t}\int \frac{1}{2}\left[u_g^2 + v_g^2 + \left(\frac{\theta_g}{N}\right)^2\right] dV = \left(\frac{f}{N}\right)\Lambda \int v_g\left(\frac{\theta_g}{N}\right) dV, \tag{2}$$

where for simplicity constant shear and stratification have been assumed. From (2) it can be seen that total perturbation energy growth is due solely to positive meridional heat flux, which converts available potential energy (APE) from the basic state to the perturbations.

By appealling to Schwartz's inequality we have

$$\frac{\partial}{\partial t}\int E_{qg}\,dV \le \left(\frac{f}{N}\right)\Lambda \int \frac{1}{2}\left[v_g^2 + \left(\frac{\theta_g}{N}\right)^2\right] dV \le \left(\frac{f}{N}\right)\Lambda \int E_{qg}\,dV, \tag{3}$$

and therefore,

$$\frac{1}{\int E_{qg}\,dV}\frac{\partial \int E_{qg}\,dV}{\partial t} \le \left(\frac{f}{N}\right)\Lambda. \tag{4}$$

Thus, the maximum QG energy growth rate cannot exceed $(f/N)\Lambda$, which, for typical midlatitudinal-tropospheric values of $f = 10^{-4}\ \mathrm{s}^{-1}$, $N = 10^{-2}\ \mathrm{s}^{-1}$, gives an upper bound on the energy growth rate of 10^{-2} times the shear.

On the other hand, the total energy growth in PE can be shown [using (1)] to be

$$\begin{aligned}\frac{\partial}{\partial t}\int E\,dV &= \frac{\partial}{\partial t}\int \frac{1}{2}\left[u^2 + v^2 + w^2 + \left(\frac{\theta}{N}\right)^2\right] dV \\ &= \Lambda \int \left[\left(\frac{f}{N}\right)v\left(\frac{\theta}{N}\right) - uw\right] dV \\ &\le \Lambda \int \frac{1}{2}\left\{\left(\frac{f}{N}\right)\left[v^2 + \left(\frac{\theta}{N}\right)^2\right] + u^2 + w^2\right\} dV \\ &\le \Lambda \int E\,dV,\end{aligned} \tag{5}$$

and therefore,

$$\frac{1}{\int E\,dV}\frac{\partial \int E\,dV}{\partial t} \le \Lambda. \tag{6}$$

Hence, the theoretical upper bound on PE energy growth rate is N/f times the upper bound on energy growth rate in QG. Inequalities (4) and (6) indicate that the kinetic energy (KE) shear mechanism could be much more effective than the conventional APE mechanism in transferring energy from the mean flow to the perturbations. In other words, perturbation growth may be dominated by the momentum flux mechanism, which directly reduces the mean shear, rather than by the heat flux mechanism, which reduces the mean shear indirectly (by reducing the temperature gradient that maintains the shear). A scale analysis presented below suggests that the KE shear term could dominate when the perturbation horizontal scale is smaller than 1000 km. This raises the fundamental question of why most variance is observed to be baroclinic in origin and at synoptic scale. In fact we find that temporally and spatially white stochastic forcing would maintain comparable variance in the balanced and gravity wave modes suggesting that it is the nature of the forcing and the enhancement of damping associated with turbulent interactions rather than the potential for perturbation growth and persistence that explains the observed dominance of approximately balanced modes.

c. The nongeostrophic Eady model

Consider the Eady (1949) model for the midlatitude troposphere consisting of a mean zonal wind that increases linearly with height $\overline{U}(z) = \Lambda z$ between two horizontal solid boundaries at $z = 0$; H. As in the unbounded shear problem above, an f plane, constant stratification, and the Boussinesq approximation are assumed. Characterizing the Eady model are the following quantities: the tropopause height H, which provides the

scale for distance in the vertical, the vertical shear Λ (and thus the scale for horizontal velocity ΛH), the stratification N, and the rotational timescale f^{-1} (corresponding to 2.8 h per nondimensional time unit for $f = 10^{-4}\ \mathrm{s}^{-1}$, which will be assumed). A horizontal scale L is not imposed by the model and one could be chosen arbitrarily. Here, we adopt the conventional scaling by the Rossby radius of deformation $L = NH/f$;[1] however, perturbation dynamics with larger and smaller scales than the Rossby radius will be investigated as well. Using f, H, L to nondimensionalize (1) results in

$$\frac{d\tilde{u}}{d\tilde{t}} = \tilde{v}_a - S\tilde{w}, \tag{7a}$$

$$\frac{d\tilde{v}}{d\tilde{t}} = -\tilde{u}_a, \tag{7b}$$

$$\alpha^2\frac{d\tilde{w}}{d\tilde{t}} = -\tilde{\phi}_{\tilde{z}} + \tilde{\theta}, \tag{7c}$$

$$\frac{d\tilde{\theta}}{d\tilde{t}} = S\tilde{v} - \tilde{w}, \tag{7d}$$

$$\tilde{u}_{a\tilde{x}} + \tilde{v}_{a\tilde{y}} + \tilde{w}_{\tilde{z}} = 0, \tag{7e}$$

where the tilde denotes nondimensional variables; the linearized substantial derivative is $d/d\tilde{t} = \partial/\partial\tilde{t} + \tilde{z}S(\partial/\partial\tilde{x})$, the shear number is defined as $S = 1/\sqrt{\mathrm{Ri}} = \Lambda/N$, and $\alpha = H/L$ denotes the aspect ratio. We hereafter approximate (7c) by assuming quasi-hydrostatic balance $\tilde{\theta} = \tilde{\phi}_{\tilde{z}}$, which is valid when $\alpha^2 \ll 1$. Thus, we cannot address perturbation dynamics for disturbances with horizontal scale equal to or smaller than the associated vertical scale. Eady (1949) suggested transforming (7) into a set of three equations for the three variables: vertical component of relative vorticity, vertical velocity, and the Laplacian of the potential temperature. He also showed how (7) can be written as a single third-order equation for the vertical velocity. In this study, however, we choose to separate the geostrophic and nongeostrophic contributions as much as possible. Therefore, we transform (7) into the following set (hereafter we omit the tilde superscript):

$$\frac{d}{dt}v_{az} = -2Sv_x + (w_x - u_{az}), \tag{8a}$$

$$\frac{d}{dt}u_{az} = 2Sv_y - (w_y - v_{az}), \tag{8b}$$

$$\frac{d}{dt}(v_x - u_y + \theta_z) = S(w_y + v_{az}), \tag{8c}$$

in which $\mathbf{u} = \mathbf{u}_g + \mathbf{u}_a$, and the perturbation geostrophic components satisfy the thermal wind relations $v_{g_z} = \theta_x$, $u_{g_z} = -\theta_y$. In the QG limit the lhs of (8a) and (8b) vanish and these equations become the linearized version of the **Q**-vector diagnostic equations (Hoskins et al. 1978), which assume a perfect balance between advection of mean meridional temperature by the geostrophic velocity and the response of adiabatic heating/cooling by the induced ageostrophic circulation. However, in the nongeostrophic dynamic regime, the imbalance between those two terms forces the tendency of the ageostrophic wind. On the rhs of the potential vorticity (PV) equation (8c), Sw_y tilts the horizontal mean vorticity into the vertical by differential vertical advection of the mean zonal wind. The second term, Sv_{az}, alters the thermal component of the PV due to vertical differential advection of the mean temperature by the ageostrophic velocity. In the QG limit, both terms vanish.

[1] This is equivalent to setting $\mathrm{Bu} = \mathrm{RiRo}^2 = 1$, where $\mathrm{Bu}, \mathrm{Ri} = (N/\Lambda)^2$, and $\mathrm{Ro} = U/fL = \Lambda H/fL$, are the Burger, Richardson, and Rossby numbers, respectively.

3. Generalized stability analysis

a. The energy norm

We choose the total energy inner product to measure perturbation magnitude. Energy provides a convenient and physically interpretable norm while (potential) enstrophy does not because in the absence of shear the gravity wave modes have zero PV, which is also true for the QG Eady normal modes. It follows that the enstrophy inner product does not possess the positive definiteness required to generate a norm. In addition, the nonnormal energetics that occur in the presence of shear play a central role in our study, which further motivates the choice of the energy norm.

We apply the 3D Helmholtz decomposition, suggested by Muraki et al. (1999), on (8) in order to separate the ageostrophic component from the geostrophic one. Then (8) can be written as

$$\frac{\partial \boldsymbol{\chi}}{\partial t} = \mathbf{D}\boldsymbol{\chi}, \tag{9}$$

where $\boldsymbol{\chi}$ is the generalized energy coordinates vector, and the matrix $\mathbf{D}$ results from the energy coordinate transformation of (8) (details are given in appendix A).

We study both the inviscid version of the Eady model and the viscid version (appendix B). The inviscid version of this model is singular and its continuous spectrum is composed of singular modes, while with vertical diffusion however small the model is nonsingular and the singular modes of the inviscid problem are replaced by a discrete spectrum of analytic modes. The exponentially stable and unstable modes that are the objects of study in traditional modal stability analysis are analytic both in the inviscid and the viscous problems and do not become singular with the vanishing of viscosity as the singular spectrum does, so it is not necessary in performing a modal stability analysis to take care that the entire spectrum of modes is physically sensible. However, GST applied to the inviscid problem traces energy growth in large part to interaction among the

singular continuous spectrum and the analytic normal modes. However, the singular spectrum, which is composed of a real number infinity of singular modes, can in no sense be placed in correspondence with the countable discrete analytic modes of the physical viscous problem, no matter how small the viscosity. For this reason results obtained using the inviscid analysis insofar as these results pertain to the study of modal decomposition and projections must be verified in the presence of small diffusion in which case the interaction is among physically realistic discrete analytic modes that have no counterpart in the continuous spectrum of singular modes. If one is interested in studying the manifolds of approximately balanced rotational geostrophic modes and the gravity modes and especially in their nonorthogonality and interactions in the presence of shear, which result in mutual excitation, it is necessary to study the physical viscous problem. However, the integrated results of initial value problems with analytic initial conditions approach asymptotically the same solution in the viscous and inviscid problems as the viscosity decreases so if one is interested in, for example, obtaining optimals, which are smooth initial conditions, the inviscid problem offers important computational economies, although its underlying modal structure is not physical.

We begin with an investigation of the instantaneous perturbation energy growth and continue with optimal excitation analysis for an intermediate time; we end this section by referring to the optimal excitation for the asymptotic $t \to \infty$ limit.

b. Instantaneous growth

The maximum instantaneous growth rate of system (9) is equal to the largest eigenvalue of the matrix $(\mathbf{D} + \mathbf{D}^\dagger)/2$, and the structure $\boldsymbol{\chi}$ producing this growth rate is its associated eigenvector (FI96). We assume a horizontal Fourier decomposition of the solution spacial structure $\boldsymbol{\chi} = \tilde{\boldsymbol{\chi}}(z, t)e^{i(kx+ly)}$, where k, l are the scaled zonal and meridional wavenumbers. Then the instantaneous growth rate of $\boldsymbol{\chi}$ for symmetric horizontal plane waves $k = l$ and scaled by the timescale for horizontal advection $(f/N)\Lambda$ as a function of the zonal wavenumber nondimensionalized by the the horizontal space scale $(N/f)H$ is shown in Fig. 1.[2]

The solid line indicates the most unstable normal mode growth rate of the classical QG Eady model, while the dashed line shows the maximal instantaneous QG growth rate. As expected from the QG energy growth rate bound (4), the QG growth rate does not exceed the scaled value 0.5, that is, $(f/N)\Lambda/2$ (the instantaneous growth rate of $\boldsymbol{\chi}$ is half the instantaneous energy growth rate). In contrast the circled symbols indicate the instantaneous growth rate obtained from the PE solution,

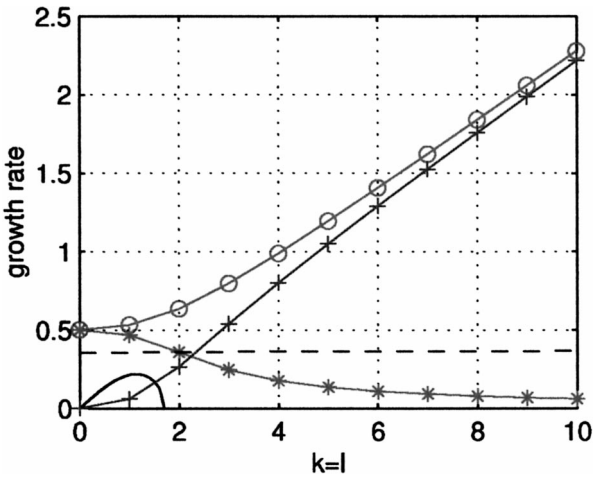

FIG. 1. The maximum instantaneous growth rate that can be obtained by symmetric perturbations under PE dynamics in the Eady model is indicated as a function of horizontal plane wavenumber $k = l \in (0, 10)$ by the circles. The APE contribution to the growth, $v\theta/2$ is indicated by the asterisks, and the KE shear term contribution $-uw/2$ by the plus signs. For comparison, the maximum instantaneous growth rate that can be obtained under QG dynamics is indicated by the dashed line and the unstable QG normal mode growth rate by the solid line. Growth rate is scaled by $(f/N)\Lambda$; the wavenumber k is scaled by $(N/f)H$.

which increases dramatically with wavenumber, from scaled values of 0.5 as $k = l \to 0$. This growth rate is composed of a contribution from the APE growth term $v\theta/2$, as indicated by the asterisks, and a contribution from the KE shear term $-uw/2$, as indicated by the plus symbols. We can see that the APE mechanism dominates at small wavenumbers, but as k exceeds 2.25, corresponding to a cyclone with a half-wavelength of approximately 1000 km, the shear term begins to dominate so that, as k reaches 10, nearly all of the instantaneous growth arises from the KE shear term. The dependence of energetics on wavenumber is shown in Fig. 1 for the shear $S = 0.1$ corresponding to Ri = 100; however, the result in Fig. 1 is insensitive to the Richardson number [over the range $O(10^{-4}) \le \text{Ri} \le O(10^4)$]. It is also insensitive to the addition of small amounts of vertical diffusion to the model in order to regularize the modes.

The question of whether the system is able to maintain such large growth, or whether it is a short-term phenomena, is examined next.

c. Intermediate time optimal growth

The solution of (9) can be written as

$$\boldsymbol{\chi}(t) = e^{\mathbf{D}t}\boldsymbol{\chi}(0) = \mathbf{U}\boldsymbol{\Sigma}\mathbf{V}^\dagger\boldsymbol{\chi}(0), \tag{10}$$

where $\mathbf{U}\boldsymbol{\Sigma}\mathbf{V}^\dagger$ is the singular value decomposition (SVD) of the matrix propagator from an initial time zero to target time t, $\boldsymbol{\Phi}(0, t) = e^{\mathbf{D}t}$, in which $\mathbf{U}$ and $\mathbf{V}$ are two unitary matrices, $\boldsymbol{\Sigma}$ is a diagonal matrix with positive elements ordered by growth (cf. Noble and Daniel 1988; FI96), and the dagger denotes the Hermitian transpose.

[2] We restrict ourselves to the wavenumber range $0 < k \le 10$ in which the hydrostatic approximation is valid.

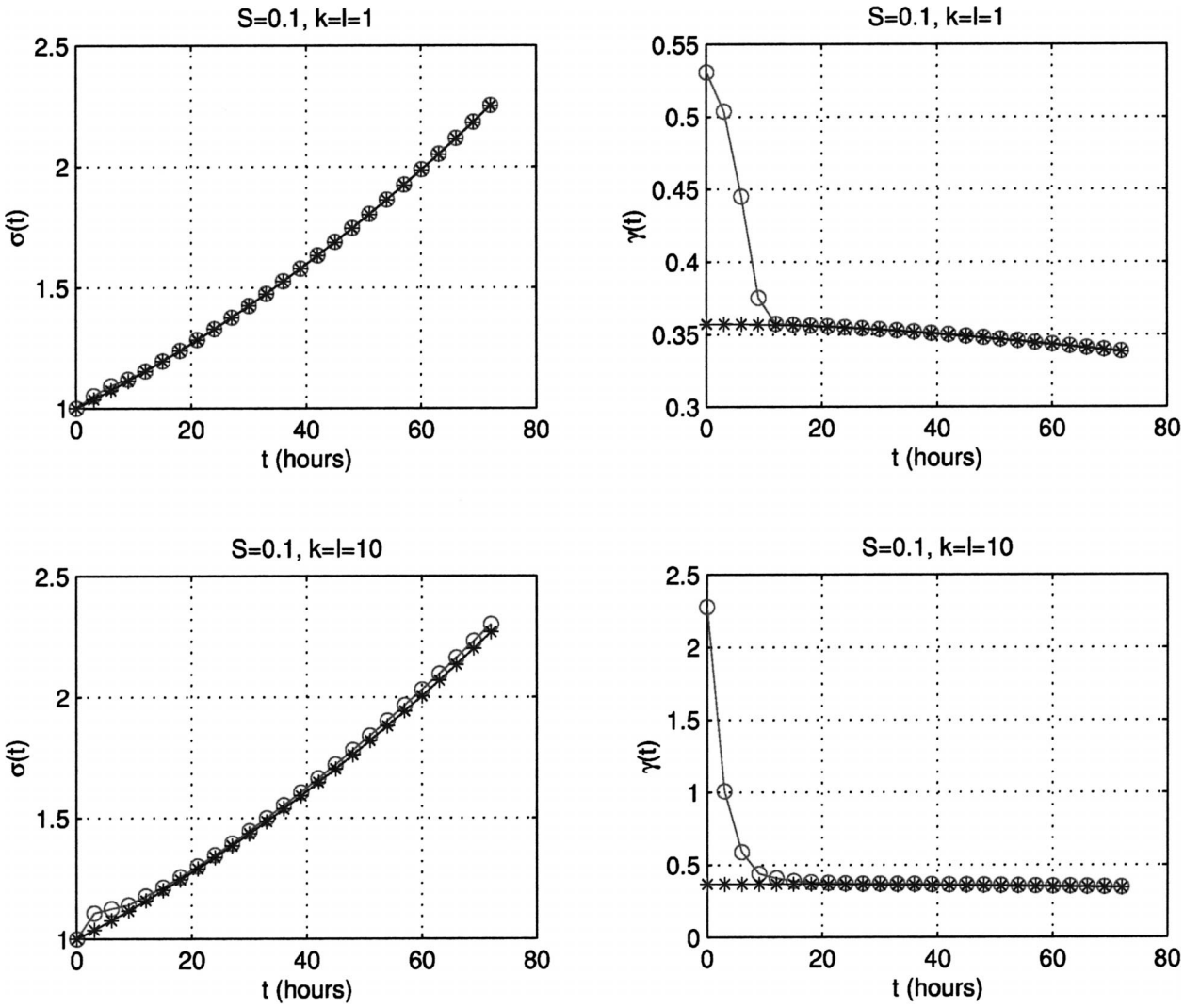

FIG. 2. (top left) The optimal growth of $\sigma(t)$ obtained over time interval t by symmetric wavenumber perturbations; $k = l = 1$ in the Eady model with shear $S = 0.1$; (top right) the corresponding effective growth rate $\gamma(t) = \ln\sigma(t)/t$, scaled by $(f/N)\Lambda$. For both left and right, the PE growth is indicated by circles, and the QG growth rate by asterisks. (bottom) Same as in the top but for $k = l = 10$.

We identify the optimal initial unit magnitude perturbation $\boldsymbol{\chi}(0)$ producing maximal growth at target time t to be the first column vector of $\mathbf{V}$ that is projected by $\boldsymbol{\Phi}(0, t)$ onto the first column unit vector of $\mathbf{U}$ with magnitude increase $\sigma = \Sigma_{11}$, where σ denotes the optimal growth over time t.

We analyze next the optimal growth and the associated structures for the shear number $S = 0.1$ (Ri = 100), focusing on two characteristic wavenumbers $k = 1, 10$, corresponding to synoptic- and subsynoptic-scale structures.

1) GROWTHS AND STRUCTURES

The finite time optimal growth properties are shown in the top of Fig. 2 for the synoptic-scale waves and in the bottom for the subsynoptic-scale waves. Circles indicate the PE solution and the asterisks indicate the QG solution with the same shear number. The optimal growth $\sigma(t)$ over the interval of time t is shown at the left. The mean growth rate $\gamma(t)$, for these optimals, satisfying $\sigma(t) = \exp(\gamma t)$, where $\gamma(t)$ is normalized by $(f/N)S$, is shown at the right. We see that although the optimal instantaneous PE growth rate is considerably larger than the optimal instantaneous QG growth rate in the synoptic scale and enormously larger in the subsynoptic scale, the optimal growth attained for times larger than 3 h (the nondimensional time unit is $1/f$) in PE is almost identical to the optimal growth attained in the QG analysis.

The evolution of the integrated heat and momentum fluxes for a 2-day optimal (not shown here) indicates that the evolution is almost purely on the geostrophic manifold and the growth is almost completely due to the geostrophic component of meridional heat flux (the

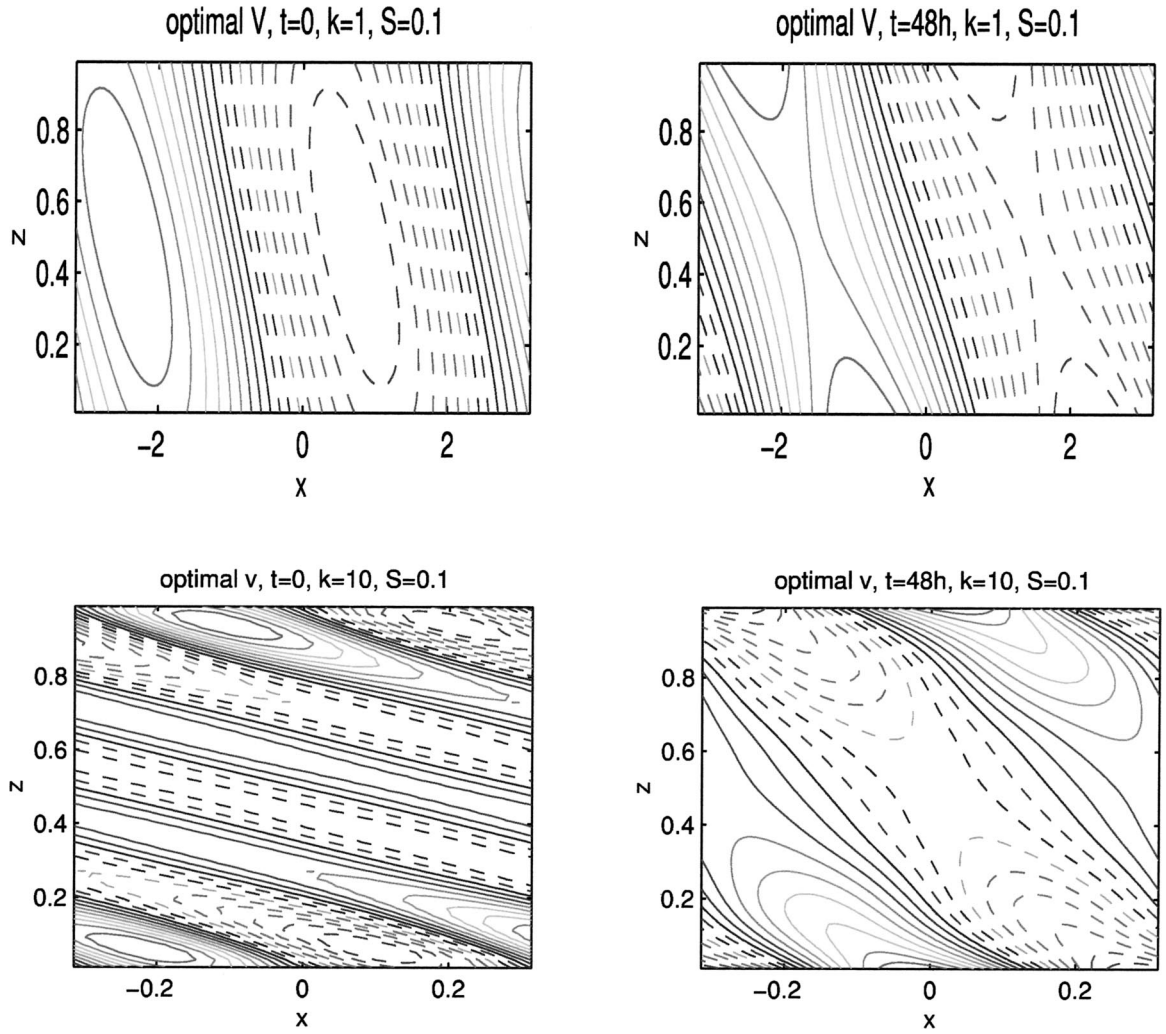

FIG. 3. (top) Zonal-vertical cross sections of the (left) initial and (right) final meridional wind v for the 2-day optimal in the Eady model with $k = l = 1$. (bottom) Same as the top, but for $k = l = 10$.

total heat flux matches almost exactly the flux obtained by the QG dynamics). The zonal-vertical cross sections of the initial and final meridional wind for the 2-day optimal are shown at the top of Fig. 3 for the synoptic scale and in the bottom for the subsynoptic scale. In agreement with the above, these structures are indeed almost identical to the QG optimal structures.

In order to better understand these results we consider next the dispersion relation and the amount of orthogonality between the divergent and rotational modes.

2) DISPERSION RELATION AND MODAL ORTHOGONALITY

The inviscid dispersion relation is shown in Fig. 4 (top) where circles indicate the ω values of the two QG normal modes. For the synoptic scale (left) we can see three distinct branches where the left and the right branches are slightly modified versions of the Poincarè modes in the absence of shear (taking into account the Doppler shift $kS/2 = 0.05$ due to the averaged mean zonal wind).[3] On the other hand, the middle branch contains two normal modes, which are almost identical to the QG normal modes, and also a spectrum of singular neutral modes, with steering levels within the domain, where $\omega_r/f \in \pm(0, kS)$ for these modes. In the subsy-

[3] The Poincarè waves, which are the inertio-gravity waves in the absence of shear, satisfy

$$\frac{\partial^2}{\partial t^2} w_{zz} + \nabla^2 w = 0$$

(∇^2 is the 3D Laplacian), which is the nondimensional version in Gill (1982, p. 258). The horizontal boundaries of the Eady channel force w to vanish there, and thus a wavelike solution of the form $w = \hat{w}(z) \exp^{i(kx+ly-\omega t)}$ should satisfy $\hat{w}(z) \propto \sin[\pm K/(\sqrt{\omega^2 - 1})z]$ with the dispersion relation $\omega = \pm\sqrt{K^2 + (n\pi)^2}/n\pi$, where n is an integer. This solution differs from the unbounded free wave solution by being untilted and by having a discrete vertical wavenumber.

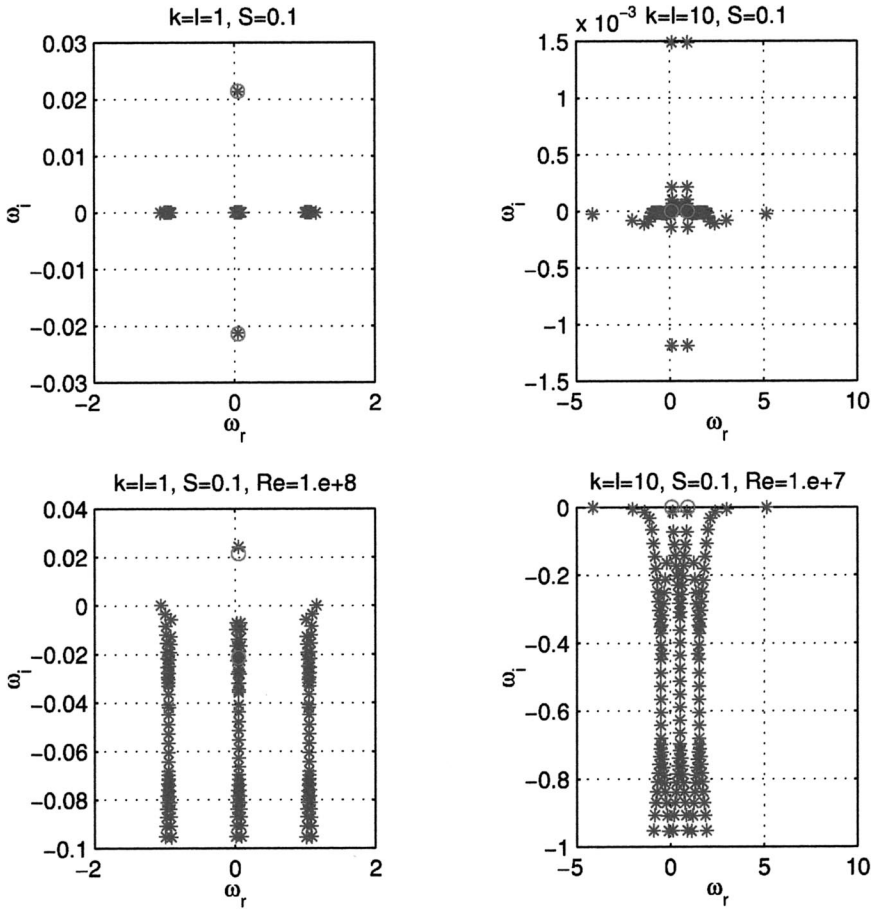

FIG. 4. (top) The inviscid PE dispersion relation for (left) $k = l = 1$ and for (right) $k = l = 10$. The frequencies ω_r, ω_i have been scaled by the Coriolis parameter f. The circles indicate growing and decaying normal modes obtained from QG dynamics. (bottom) Same as the top, except for viscid dynamics with Reynolds number Re $= O(10^8; 10^7)$, corresponding, respectively, to $k = l = 1;10$.

noptic scale (right) the right and the left branches have the nonsheared Poincarè's frequency range (shifted by $kS/2 = 0.5$), where for the middle branch the range of the rotational mode's frequency lies within ($0 < kS < 1$). Hence, although the frequencies of the Poincarè modes approach the rotational one [as expected when Ro $= O(1)$], they do not overlap.

The small instability obtained by the rotational modes in the subsynoptic scale is due to the presence of critical layers in the inviscid PE Eady model, which yield the appearance of singular modes (Nakamura 1988). The singular modes are resolved and the rotational instability vanishes when a small viscosity is added (Fig. 4, bottom).[4] Since diffusion is proportional to the second derivative in z, the Poincarè waves, as well as the rotational discrete modes, decay in proportion to the square of their vertical wavenumber.

Ordering the modes according to their frequency values in increasing order (so that the mode with the index $i = 1$, corresponds to the mode with the smallest frequency) then a contour plot of $\mathcal{E}_{i,j} = \boldsymbol{\chi}_i^\dagger \boldsymbol{\chi}_j$, at the intersection of ($x = i$, $y = j$), where $\boldsymbol{\chi}_i$ is the normalized generalized coordinate vector of mode i, so that $\boldsymbol{\chi}_i^\dagger \boldsymbol{\chi}_i = 1$, is shown in Fig. 5 (top). This contour value is a measure of energy orthogonality among the modes, and we see that in both the synoptic and the subsynoptic scales the divergent modes are almost orthogonal to each other[5] and to the rotational modes.[6] However, the rotational singular modes and the two normal modes are not orthogonal, as in QG dynamics (Farrell 1984). The presence of viscosity increases the nonorthogonality within each branch [Fig. 5 (bottom)]; however, the di-

[4] The smallest viscosity required to resolve the modes was found to yield, respectively, Reynolds number at the order of $O(10^8; 10^7)$, for the scaled wavenumber $k = 1$, 10 (see appendix B).

[5] It can be shown that in the limit of zero shear case the Poincarè waves in the Eady channel are perfectly orthogonal to each other with respect to the energy norm.

[6] In the limit of zero shear it was also shown by Bluemen (1975) that the rotational and the divergent modes are orthogonal.

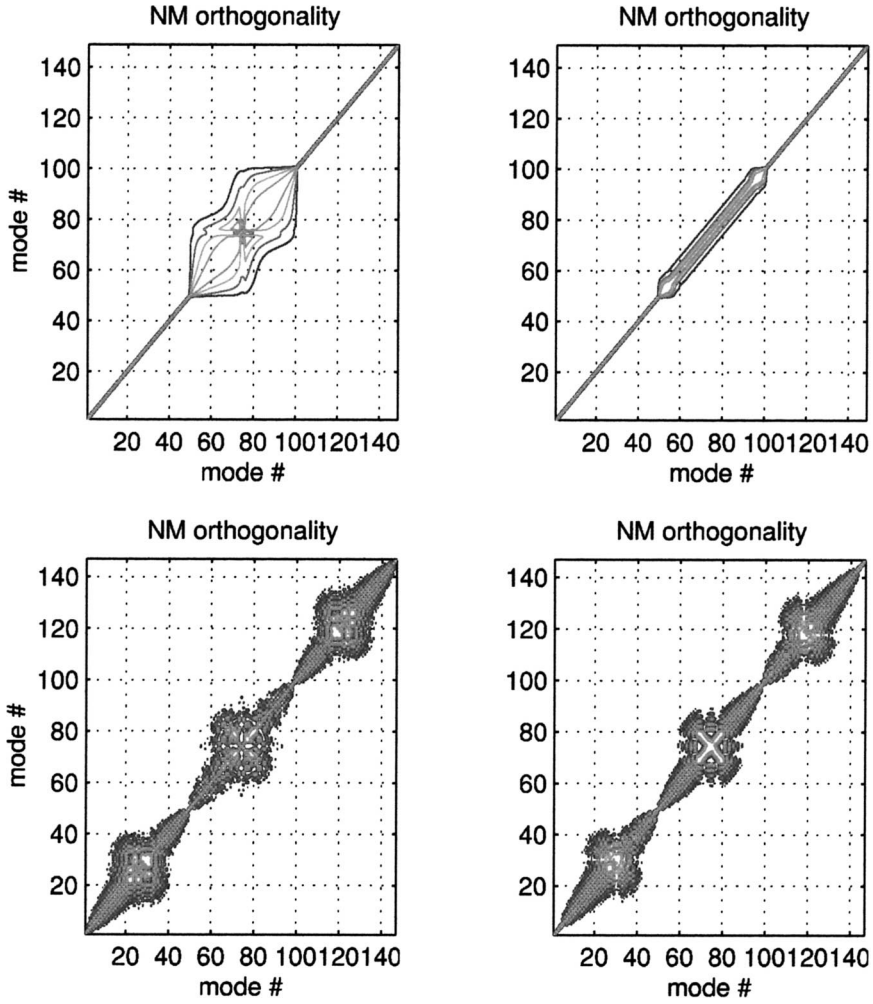

FIG. 5. (top) A contour plot indicating the relative orthogonality among modes for (left) $k = l = 1$ and (right) $k = l = 10$. It shows contours of $\mathcal{E}_{i,j} = \boldsymbol{\chi}_i^\dagger \boldsymbol{\chi}_j$, at the intersection of ($x = i$, $y = j$), where $\boldsymbol{\chi}_i$ is the normalized energy coordinate vector of mode i, (ordered by their frequency values) so that $\boldsymbol{\chi}_i^\dagger \boldsymbol{\chi}_i = 1$. (bottom) Same as the top, except for viscid dynamics with Reynolds number Re $= O(10^8; 10^7)$, corresponding, respectively, to $k = l = 1;10$.

vergent modes remain nearly orthogonal to the rotational modes.

To summarize, we see a clear separation between modes that are almost purely divergent and modes that are almost purely rotational. The typical shear number in baroclinic jets is too small to give rise to a substantial amount of nonorthogonality between the branches and therefore the divergent unbalanced modes do not project strongly onto the ''balanced QG slow manifold dynamics.''[7] Hence, for typical timescale of cyclone development (12–48 h), QG dynamics provide an accurate approximation to PE dynamics. The potentially highly effective growth mechanisms, which are filtered out by the QG approximations, are important only for the first few hours of evolution, but are not sustained and thus become irrelevant to the synoptic timescale.

In order to complete the GST analysis, we investigate next the optimal evolution for target time infinity.

d. The asymptotic $t \to \infty$ optimal

The optimal excitation for $t \to \infty$ target time is the perturbation that optimally excites the dominant mode, which can be the most unstable, neutral, or the least damped mode, respectively, to the cases of instability, neutrality, or stability. It is the conjugate of the biorthogonal vector of the dominant mode. In the case of the inviscid Orr–Somerfeld equations this perturbation is concentrated in the region of the critical level, and is exactly proportional to $\boldsymbol{\chi}(t = \infty)/[\overline{U}(z) - c]$, where $\boldsymbol{\chi}(t = \infty)$ is the most unstable normal mode with the phase speed c (Drazin and Reid 1981, section 21). Although

[7] For intermediate and small Richardson numbers, the interaction can be very different, as will be shown in Part II (not yet submitted to *J. Atmos. Sci.*).

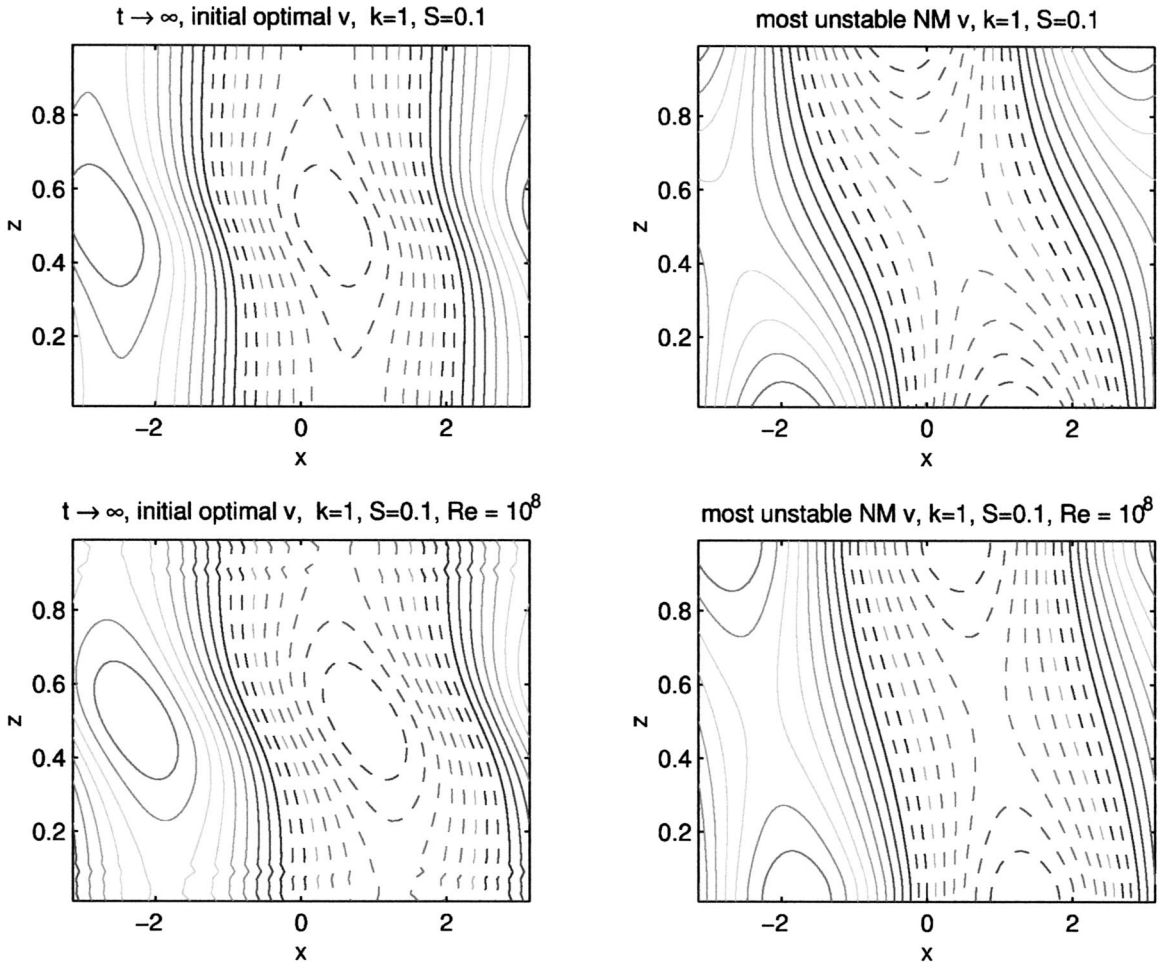

FIG. 6. (top) Zonal-vertical cross sections of the meridional wind v for the (left) optimal and (right) evolved optimal for target time infinity in the inviscid Eady model with $k = l = 1$. (bottom) Same as the top, but for the viscid dynamics.

the functional form of this optimal in our problem is not as simply expressed, it will be seen that the optimal structure in this case is also concentrated in the region of the critical layer. If the instability is small, that is, if the imaginary part of c is small, we expect to find the initial optimal concentrated in the vicinity of the critical level.

The meridional wind zonal-vertical cross sections of the initial optimal for time infinity, and of the most unstable normal mode, for $k = 1$, are shown in Fig. 6 (top). Structures for the same case, except in the presence of small viscosity, are shown in Fig. 6 (bottom). The structures are almost purely geostrophic and are almost identical to the structures obtained from QG dynamics, where the initial optimal is found to be maximized at the midtropospheric steering level and the most unstable mode is found to be maximized at the boundaries. The viscid structures are different from the inviscid ones by being slightly more smooth in vertical structure confirming the convergence of smooth initial conditions despite the complete difference in the mode structure between these two representations. Note also that the optimal excitation for the mode differs markedly in structure from the mode itself and that it exhibits the familiar concentration of the optimal perturbation in the region of the critical layer characteristic of zonally symmetric model problems.

The meridional wind structures for the subsynoptic-scale case $k = 10$ are shown in Fig. 7. The two most unstable rotational modes are equally unstable, with critical layers located within the domain, one near the ground and the other near the tropopause. The former mode is chosen for display in Fig. 7 (top right). Although the presence of explicit ageostrophic dynamics in the PE framework destabilize the neutral QG Eady modes, their structure remains almost purely geostrophic, gaining a slight tilt. The instability of this mode is slight, and the optimal initial excitation is correspondingly highly concentrated in the vicinity of the critical layer (Fig. 7, top left). In the presence of small viscosity all modes become damped, but the least damped modes become the two divergent modes with the smallest and

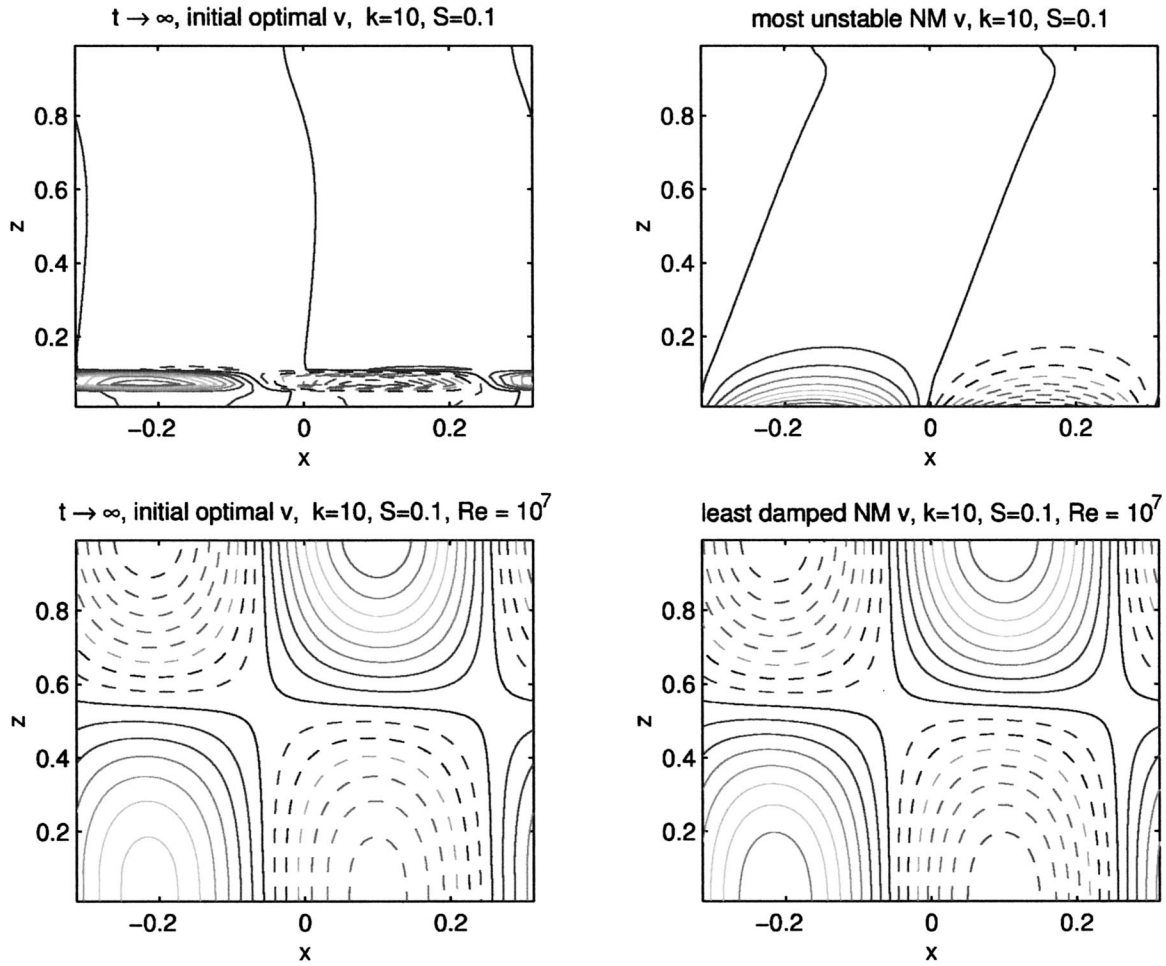

FIG. 7. Same as in Fig. 6, but for the $k = l = 10$ case.

largest frequencies (and with steering levels outside the flow). The structure of these modes are almost identical to that of the pure Poincarè modes with vertical wavenumber ± 1. These two modes are almost orthogonal to all other modes, and therefore their biorthogonal vectors are nearly identical with the modes themselves as can be seen in Fig. 7 (bottom) where the mode with positive wavenumber has been chosen for display.

The above analysis of the optimal linear excitation for target time infinity is a limiting case shown in part because of its simplicity in that the optimal way to excite the most unstable mode is its biorthogonal conjugate. In order to assess the relevance of this limit we need to find the minimal target time required for the optimal excitation to converge to the asymptotic $t \to \infty$ optimal. For the inviscid $k = 1$ case this minimal target time is found to be 15 days, and about 20 days for the viscid case (recalling that there are 2.8 h per nondimensional time unit). When $k = 10$, the minimal times are 60 and 30 days for the inviscid and the viscid cases, respectively. (The large difference between the latter is due to the fact that the least damped divergent mode in the presence of viscosity is entirely different in structure from the most unstable rotational mode obtained by the inviscid dynamics.) As the characteristic timescale for extratropical cyclone development is of the order of a day or two, these limiting cases are unlikely to be observed.

Although including explicit divergent dynamics has little effect on the development of balanced motions, the enhanced growth produced by the PE dynamics and the existence of modal divergent structures in the shear flow together suggest that the divergent modes might respond strongly to an equivalent stochastic forcing that parameterizes both from nonlinear interaction among waves in the flow and processes such as latent heat release (FI96). Since the statistical equilibrium of the midlatitudinal troposphere has been successfully modeled as an asymptotically stable linear dynamical system exposed to stochastic forcing (Farrell and Ioannou 1995, hereafter FI95), it is of interest to examine the response of the PE to such stochastic forcing.

4. Response to stochastic forcing

Adding a forcing vector $\mathbf{f}(t)$ to (9) yields

$$\frac{\partial \boldsymbol{\chi}}{\partial t} = \mathbf{D}\boldsymbol{\chi} + \mathbf{f}(t) \tag{11}$$

with solution in the frequency domain

$$\hat{\boldsymbol{\chi}}(\omega) = \hat{\mathbf{R}}(\omega)\hat{\mathbf{f}}(\omega) \tag{12}$$

in which appears the resolvent

$$\hat{\mathbf{R}}(\omega) = (i\omega\mathbf{I} - \mathbf{D})^{-1} \tag{13}$$

in which the hat denotes the Fourier transform

$$\hat{\boldsymbol{\chi}}(\omega) = \frac{1}{2\pi}\int_{-\infty}^{\infty} \boldsymbol{\chi}(t)e^{-i\omega t}\, dt, \tag{14}$$

where ω is the frequency and $\mathbf{I}$ the identity matrix.

Using the SVD of the resolvent $R = \mathbf{U}\boldsymbol{\Sigma}\mathbf{V}^{\dagger}$ and assuming for a given ω an ensemble of spatially uncorrelated forcings with unit variance, that is, $\langle \hat{\mathbf{f}}_i, \hat{\mathbf{f}}_j^{*} \rangle = \delta_{ij}$, the ensemble average covariance matrix of $\hat{\boldsymbol{\chi}}$ at a given ω can be written as

$$\mathbf{C}(\omega) = \hat{\boldsymbol{\chi}}\hat{\boldsymbol{\chi}}^{\dagger} = \mathbf{R}\mathbf{R}^{\dagger} = \mathbf{U}\boldsymbol{\Sigma}^2\,\mathbf{U}^{\dagger}. \tag{15}$$

Hence, the column vectors of $\mathbf{U}$ are the empirical orthogonal functions (EOFs) of $\hat{\mathbf{C}}(\omega)$. The ith EOF vector results from sinusoidal forcing with the structure of the ith column vector of $\mathbf{V}$, which can be found alternatively from SVD of the Hermitian matrix $\mathbf{B}(\omega) = \mathbf{R}^{\dagger}\mathbf{R} = \mathbf{V}\boldsymbol{\Sigma}^2\,\mathbf{V}^{\dagger}$.

When a spectrum of frequencies, $\omega \in (\omega_1, \omega_2)$, is excited by spatially and temporally uncorrelated forcing with unit variance, that is, $\langle \hat{\mathbf{f}}_i(\omega_m), \hat{\mathbf{f}}_j^{*}(\omega_n) \rangle = \delta_{ij}\delta(\omega_m - \omega_n)/2\pi$, then the EOFs and the stochastic optimals are obtained by the SVD of the matrices

$$\mathcal{C} = \frac{1}{2\pi}\int_{\omega_1}^{\omega_2} \mathbf{R}(\omega)\mathbf{R}^{\dagger}(\omega)\, d\omega = \mathbf{U}\boldsymbol{\Sigma}_{\mathcal{C}}^2\mathbf{U}^{\dagger},$$

$$\mathcal{B} = \frac{1}{2\pi}\int_{\omega_1}^{\omega_2} \mathbf{R}^{\dagger}(\omega)\mathbf{R}(\omega)\, d\omega = \mathbf{V}\boldsymbol{\Sigma}_{\mathcal{B}}^2\mathbf{V}^{\dagger}, \tag{16}$$

and the ensemble response variance is given by

$$\langle \boldsymbol{\chi}^2 \rangle = \frac{1}{2\pi}\int_{\omega_1}^{\omega_2} \mathbf{F}(\omega)\, d\omega, \tag{17}$$

where $\mathbf{F}(\omega) = \text{trace}[\mathbf{R}^{\dagger}(\omega)\mathbf{R}(\omega)] = \text{trace}[\mathbf{R}(\omega)\mathbf{R}^{\dagger}(\omega)]$. Note that unless the matrix $\mathbf{D}$ is normal $\boldsymbol{\Sigma}_{\mathcal{C}} \neq \boldsymbol{\Sigma}_{\mathcal{B}}$, and therefore in general a stochastic optimal is not uniquely related to an EOF. When all frequencies are excited equally (white noise), $\mathcal{C}$ and $\mathcal{B}$ can be directly obtained from the Lyapunov equations (FI96):

$$\mathbf{D}\mathcal{C} + \mathcal{C}\mathbf{D}^{\dagger} = -\mathbf{I}; \qquad \mathbf{D}^{\dagger}\mathcal{B} + \mathcal{B}\mathbf{D} = -\mathbf{I}. \tag{18}$$

In the presence of equal amounts of Rayleigh damping and Newtonian cooling, corresponding together to a damping rate of 2.5 days, all modes decay and $\mathbf{F}(\omega)$ is bounded. For this case $\mathbf{F}(\omega)$ for the wavenumbers $k = 1 = l$, 10 are shown in Fig. 8 with the thick gray line indicating the PE response. For the $k = l = 1$ case, which corresponds to horizontal wavelength $\lambda \approx 4400$ km, each branch of the divergent modes maintains almost the same amount of variance as the rotational modes (Fig. 8, top). The stochastic optimals and the EOFs calculated exclusively for the rotational spectrum, by using (17) over the corresponding range of ω, are found to maintain ~35% of the rotational perturbation energy. Their structures, which are almost identical to the corresponding structures obtained from the QG analysis, are shown in Fig. 9 (top). Moreover, Fig. 9 (bottom) shows that the first stochastic optimal and first EOF, when calculated exclusively for each of the divergent branches, are almost identical to each other and almost identical as well to the structures of the first and the last analytic modes that are shown in the dispersion relations in Fig. 4.

There is no evidence in observations for divergent modes with variance comparable to that of the rotational modes at synoptic scales. We studied modifications of the model in order to explore further mechanisms maintaining the divergent variance. A commonly suggested explanation for the suppression of gravity waves in the troposphere is that the waves propagate into the stratosphere where, as a result of density decrease related amplitude growth, they are ultimately dissipated; however, adding a sponge layer above in order to account for the stratosphere as a sink for the gravity waves was found to have little effect on the divergent wave variance. We traced this to the fact that a large subset of these waves have small vertical group velocity, and therefore are not strongly absorbed by the sponge. Adding drag within the boundary layer to account for increased eddy mixing was also found to have a small affect on the structure of $\mathbf{F}(\omega)$.

Since observations of gravity waves show a power-law behavior (e.g., Peixoto and Oort 1992), it follows that the forcing, which arises in part from (quadratic) nonlinear eddy interaction should also obey a power law, and therefore should be assumed red rather than white. In our model this is accounted for by a temporal correlation of the forcing. The dashed–dotted lines in Fig. 8 show the frequency response to red noise with an ω^{-2} dependence indicating that with this forcing the divergent branch variance is suppressed. Nonlinear eddy interaction not only forces the system, by constantly exciting all frequencies, but is also a mechanism that imposes damping at all frequencies (FI95). The Rayleigh damping that is added to the system represents partly physical processes such as the Ekman damping and Newtonian cooling, and partly parameterizes this nonlinear damping. One may argue for choosing the linear damping r to be proportional to frequency so that the e-folding time of the autocorrelation remains proportional to the eddy period; this parameterization can then be tested. The dashed lines in Fig. 8 show the effect of such a damping, and the solid–dotted lines show the response where both red noise forcing and frequency

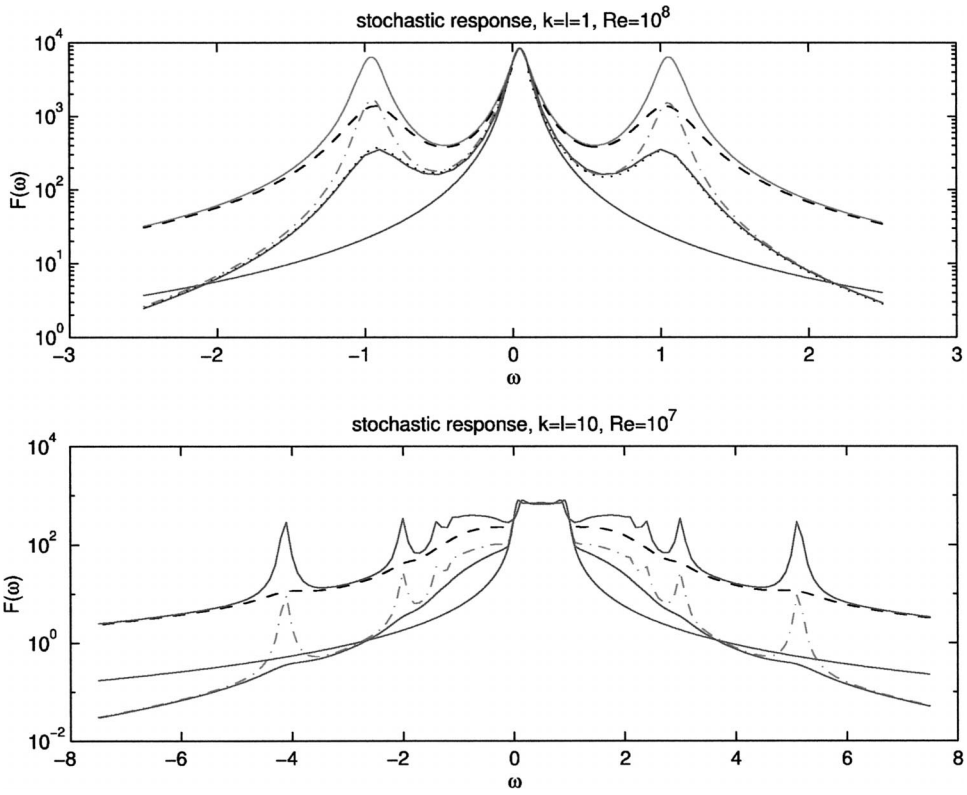

FIG. 8. Frequency response to white noise forcing (thick gray line), red noise forcing with power spectrum of ω^{-2} (dashed–dotted line), white noise with damping that increases linearly with frequency (dashed line), red noise with damping increasing linearly with frequency (solid–dotted line), and white noise in the QG framework (solid line) for (top) $k = l = 1$, and (bottom) $k = l = 10$.

dependent damping are applied. When $k = l = 10$ ($\lambda \approx 440$ km) the response of the divergent motion to white noise corresponds to almost 45% of the total variance (the thick gray line in Fig. 8, bottom), but this response is strongly suppressed when the forcing is made red (dashed–dotted line). The sharp peaks in the divergent variance that are associated with the analytic divergent modes are smoothed by linear damping (dashed line), and in combination (solid–dotted line), these reduce the divergent variance to approximately the level obtained by QG analysis (solid line). For the rotational spectrum the first stochastic optimal and the first EOF are almost identical to the corresponding structures obtained from the QG analysis (Figs. 9 and 10, top). Although the divergent variance response to white noise forcing is distributed over all the modes, the peaks associated with the analytic modes dominate the spectrum. Therefore, the first stochastic optimal and the first EOF of the divergent branches are mainly affected by those two modes (Figs. 9 and 10, bottom).

5. Discussion

This work begins a GST analysis of baroclinic shear flow using a PE. In this part we focused on the synoptic midlatitude regime, which is characterized by a Richardson number of order 100. This synoptic regime is observed to be mainly geostrophically balanced and its observed dynamics is adequately described by the QG equations.

However, it is not obvious why QG provides such a good approximation to the dynamics at high Richardson numbers. Observations and PE models indicate that synoptic eddies can be highly nongeostrophic, and theory shows that in their first few hours of evolution optimally growing perturbations experience a much larger growth than is predicted by QG. Although in their mature stage, these eddies attain a primarily geostrophic balance and their asymptotic growth rate is in general agreement with the QG prediction.

The QG framework assumes a typical perturbation spatial scale of O(1000 km) and a typical timescale of days. Therefore, the QG framework cannot address the more basic question of why the observed variance is concentrated at these spatial and temporal scales. In a PE analysis we can free the spatial scaling and explore eddies with a much wider range of spatial and temporal scales (provided only that they remain quasi-hydrostatic).

Total energy growth in a baroclinic shear flow arises both from the available potential energy source tapped by positive meridional heat flux, which acts to reduce

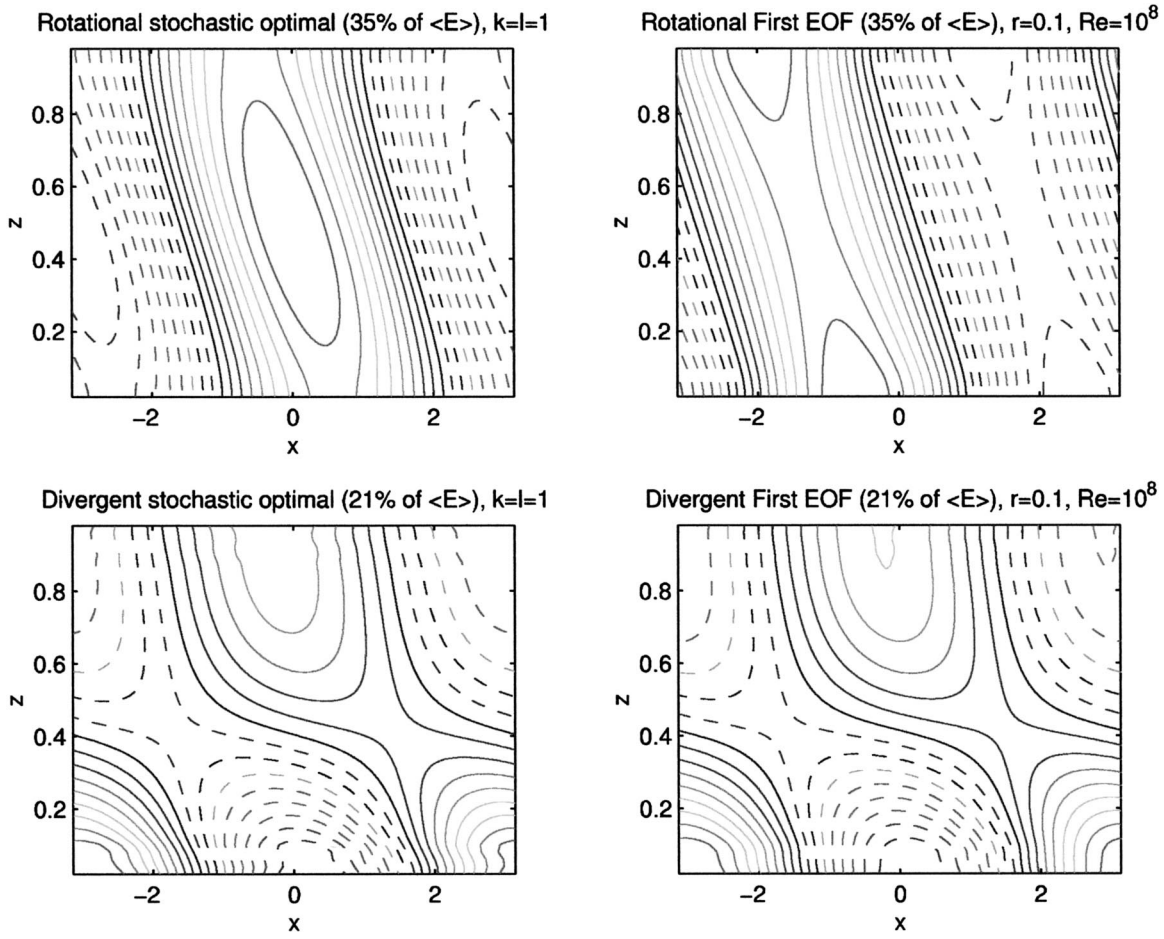

FIG. 9. (top left) The first stochastic optimal and (top right) the first EOF computed exclusively using the rotational modes. (bottom left) The first stochastic optimal and (bottom right) the first EOF computed exclusively using the gravity modes; all for the Eady model with $k = l = 1$.

the mean temperature gradient, and from the kinetic energy source tapped by downward zonal momentum flux, which acts directly to reduce the vertical shear. The latter mechanism can produce growth rate $N/f = O(10^2)$ times larger than the former; however, this kinetic energy growth mechanism is filtered out by QG. However, for eddies with scale of a few hundred kilometers the potential KE growth rate can be larger by an order of magnitude than the APE growth rate and on approaching the quasi-hydrostatic limit (aspect ratio 1), this KE growth rate can be 100 times larger than the QG growth. This result raises the question of why smaller eddies do not take advantage of this KE mechanism.

One explanation is that motions are mainly geostrophically balanced by the Rossby adjustment process, which continuously readjusts perturbations toward geostrophy by radiating the ageostophic residual portion as Poincarè waves. Since the frequency of Poincarè waves is larger than the frequency of the rotational geostrophic Rossby waves, this adjustment is approximated by QG to be instantaneous and the Poincarè waves are filtered out.

The Rossby adjustment mechanism is commonly presented for the case of zero shear, and it can be shown that in that case, the Poincarè and the Rossby waves are orthogonal. However, in the presence of shear, there is no a priori guarantee that these manifolds will remain orthogonal. Thus, there is no guarantee that perturbations cannot attain a large transient growth, filtered in QG, which is due to nonnormal interaction between these modes and the mean shear.

In order to examine these issues we explored the generalized stability of the baroclinic PE in the large Richardson number regime using the Eady model basic state in both inviscid and viscid versions, and used total hydrostatic energy to generate a norm. We showed representative results for eddies with scales of the order of 1000 and 100 km.

The instantaneous growth rate in PE was found to increase with wavenumber and to exceed the QG instantaneous growth. For cyclones with scales smaller than 1000 km, the KE growth mechanism dominates and reaches an order of magnitude larger than that obtained in QG for the mesoscale eddies. For cyclones larger than 1000 km, the APE growth dominates; how-

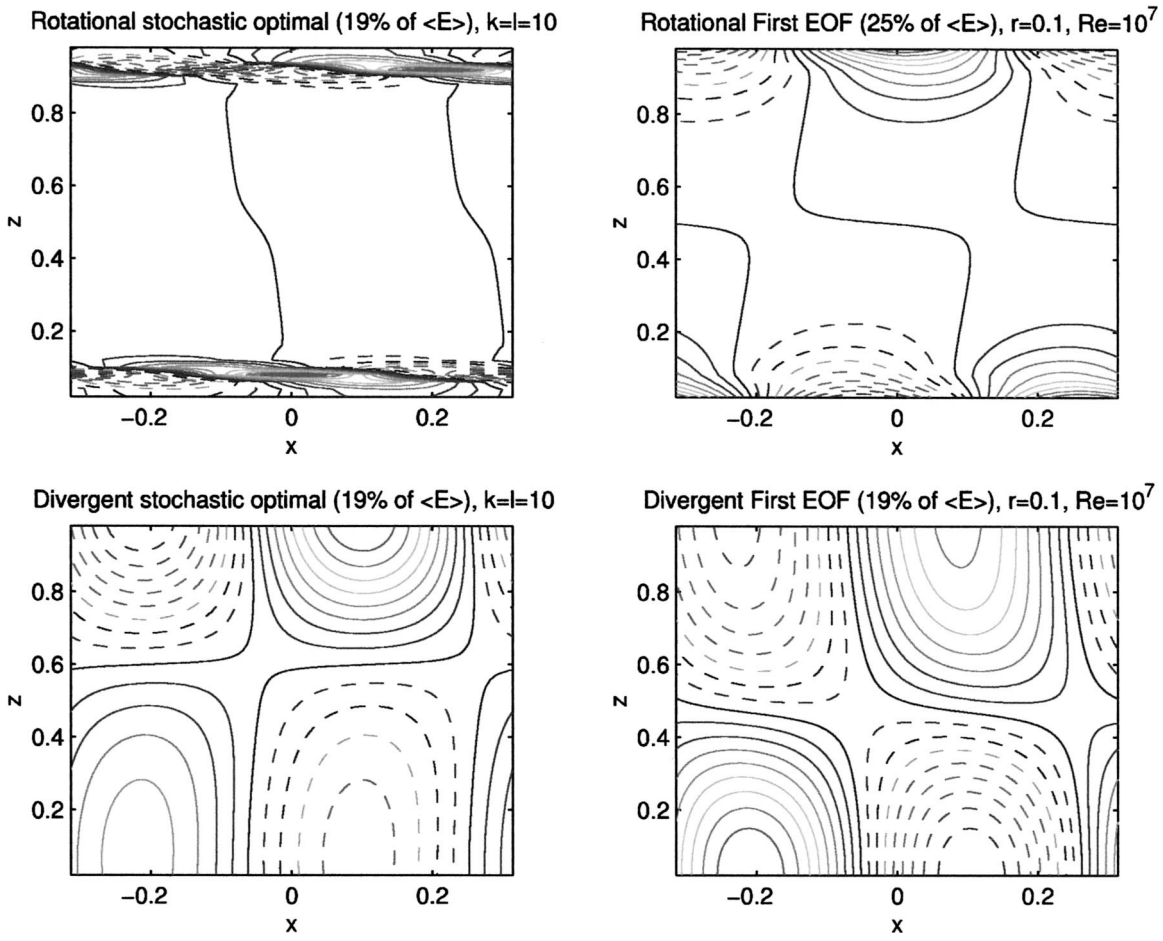

FIG. 10. Same as in Fig. 9, but for the Eady model with $k = l = 10$.

ever, the PE instantaneous growth was still found to be larger than the QG.

However, this large initial growth is not sustained for more than few hours, after which time the PE optimal growth becomes almost identical to the QG optimal growth and the evolved structures become almost purely geostrophic. The reason is that for large Richardson numbers, the divergent unbalanced manifold and the rotational balanced manifold are nearly orthogonal. Therefore, the large initial ageostrophic growth cannot be projected on and affect the evolution at the slow manifold. Orthogonality between the divergent and the rotational modes is the key to understanding why the QG approximation is so useful for large Richardson number dynamics. However, it will be shown in Part II that, as the shear increases and/or the static stability decreases, this approximate orthogonality is broken so that the divergent and rotational motions can interact more strongly.

The response of PE dynamics to white noise forcing was somewhat surprising. For the large eddies (order of 1000 km), the divergent eastward- and westward-propagating manifolds maintain variance comparable to that maintained by the rotational manifold. For the subsynoptic-scale eddies (order of 100 km) we found that the divergent manifolds maintain 45% of the total variance. There is no observational support for such strong variance in divergent large eddies. On the other hand, for mesoscale eddies, it has been shown by Koshyk et al. (1999) that high-resolution GCM simulation matched aircraft observations, which indicate that the variance of mesoscale eddies is approximately equipartitioned between the rotational and the divergent contributions. These results are in apparent agreement with ours, although it is hard to determine the Richardson number for the observed variance.

In order to examine the mechanisms supporting divergent variance, we first included in the Eady model a sponge layer above (in order to model the stratosphere as a sink for gravity waves) and a drag within the boundary layer to model boundary layer dissipation. However, because the divergent modes have small vertical group velocity, localized damping in the vertical did not affect them strongly.

On the other hand, replacing the white noise by red, which is in agreement with the power-law frequency

spectrum that is observed for gravity waves, strongly suppressed the divergent variance. Alternatively, the damping that is due to nonlinearity can be parameterized to be linearly proportional to the frequency. This makes the eddy decorrelation time proportional to the eddy period and this self-similarity is also in agreement with the observed power-law spectrum. Such a parameterized damping tends to smooth the divergent variance producing variance distribution that agree better with observations. While these considerations have not yet uniquely determined a physical explanation for the observed spectrum, the stochastic turbulence model provides a controlled setting for further investigation.

Acknowledgments. Discussions with Prof. Petros J. Ioannou have been highly informative. This work was supported by NSF Grant ATM-0123389.

APPENDIX A

Energy Norm Transformation

Applying the 3D Helmholtz decomposition, suggested by Muraki et al. (1999),[A1]

$$\begin{pmatrix} v \\ -u \\ \theta \end{pmatrix} = \nabla\Phi + \nabla \times \begin{pmatrix} F \\ G \\ 0 \end{pmatrix} = \begin{pmatrix} \Phi_x - G_z \\ \Phi_y + F_z \\ \Phi_z + G_x - F_y \end{pmatrix}, \quad \text{(A1)}$$

to (8), we obtain

$$\frac{d}{dt}[(F_x + G_y)_y - \nabla^2 G] = -2S(\Phi_x - G_z)_x + \nabla^2 F, \quad \text{(A2a)}$$

$$\frac{d}{dt}[-(F_x + G_y)_x + \nabla^2 F] = -2S(\Phi_x - G_z)_y + \nabla^2 G, \quad \text{(A2b)}$$

$$\frac{d}{dt}\nabla^2\Phi = S[2(F_x + G_y)_y - \nabla^2 G], \quad \text{(A2c)}$$

where $\nabla^2 = \partial^2/\partial x^2 + \partial^2/\partial y^2 + \partial^2/\partial z^2$. Equation (A2) can be written in the matrix form:

$$\frac{\partial}{\partial t}\hat{\boldsymbol{\eta}} = \mathbf{A}\hat{\boldsymbol{\eta}}, \quad \text{(A3)}$$

where a horizontal Fourier decomposition is assumed for the state vector $\boldsymbol{\eta} = \hat{\boldsymbol{\eta}}(z, t)e^{i(kx+ly)} = [\hat{F}(z, t), \hat{G}(z, t), \hat{\Phi}(z, t)]e^{i(kx+ly)}$; $\mathbf{A}$ is the finite difference propagator matrix, approximated by central differences of the vertical derivatives.

Boundary conditions are incorporated in $\mathbf{A}$ by noting that the vertical velocity follows from continuity (7e), which requires $w_z = (F_x + G_y)_z$, and that rigid horizontal boundary conditions satisfy $w(z = 0) = w(z = 1) = 0$, which in turn requires

$$kF(0) + lG(0) = kF(1) + lG(1). \quad \text{(A4)}$$

We choose to set

$$kF(0) + lG(0) = 0; \qquad kF(1) + lG(1) = 0, \quad \text{(A5)}$$

since this choice eliminates a zero energy subspace. Evaluated on the boundaries, the thermodynamic equation (7d) is

$$\frac{d}{dt}\Phi_z = S(\Phi_x - G_z), \quad \text{at } z = 0, 1. \quad \text{(A6)}$$

The transformation to generalized coordinates can be obtained by first writing (A1) in the matrix form:

$$\boldsymbol{\zeta} = \frac{1}{\sqrt{2}}\begin{pmatrix} v \\ -u \\ \theta \end{pmatrix} = \frac{1}{\sqrt{2}}\begin{pmatrix} 0 & -\frac{\partial}{\partial z} & \frac{\partial}{\partial x} \\ \frac{\partial}{\partial z} & 0 & \frac{\partial}{\partial y} \\ -\frac{\partial}{\partial y} & \frac{\partial}{\partial x} & \frac{\partial}{\partial z} \end{pmatrix}\begin{pmatrix} F \\ G \\ \Phi \end{pmatrix} = \mathbf{B}\boldsymbol{\eta}, \quad \text{(A7)}$$

so that the total eddy energy

$$\mathcal{E} = \boldsymbol{\zeta}^\dagger\boldsymbol{\zeta} = \boldsymbol{\eta}^\dagger(\mathbf{B}^\dagger\mathbf{B})\boldsymbol{\eta} = \boldsymbol{\eta}^\dagger\mathbf{M}\boldsymbol{\eta} = \boldsymbol{\chi}^\dagger\boldsymbol{\chi}, \quad \text{(A8)}$$

from which the generalized coordinate $\boldsymbol{\chi} = \mathbf{M}^{1/2}\boldsymbol{\eta}$ and the matrix $\mathbf{D} = \mathbf{M}^{1/2}\mathbf{A}\mathbf{M}^{-1/2}$, satisfying (9), are identified.

APPENDIX B

The PE Eady Viscid Problem

Adding vertical diffusion to the dimensional momentum and thermodynamic equations (1a), (1b), and (1d) gives

$$\frac{du}{dt} = fv_a - \Lambda w - \frac{\partial}{\partial z}\left(\nu_m\frac{\partial u}{\partial z}\right), \quad \text{(B1a)}$$

$$\frac{dv}{dt} = -fu_a - \frac{\partial}{\partial z}\left(\nu_m\frac{\partial v}{\partial z}\right), \quad \text{(B1b)}$$

$$\frac{d\theta}{dt} = f\Lambda v - N^2 w - \frac{\partial}{\partial z}\left(\nu_\theta\frac{\partial \theta}{\partial z}\right), \quad \text{(B1c)}$$

where ν_m, ν_θ are the momentum and thermal diffusivity coefficients, which we assume for simplicity to be constant and equal: $\nu_m = \nu_\theta = \nu = \text{const}$. Thus, to the rhs of the nondimensional equations (7a), (7b), and (7d) we add the terms $-\tilde{\nu}(\partial^2/\partial\tilde{z}^2)(\tilde{u}, \tilde{v}, \tilde{\theta})$, respectively, where $\tilde{\nu} \equiv S(N/f)^2\,\text{Re}^{-1}$, and $\text{Re} \equiv UL/\nu$ is the Reynolds number.

[A1] One benefit of this representation is that in the limit of zero shear the asymptotically geostrophic component $\nabla\Phi$ becomes decoupled from the asymptotically ageostrophic component $\nabla \times (F, G, 0)$, which approaches the gravity waves in this limit.

The smallest value for ν to resolve the wall boundary layer, for vertical resolution of $\delta z = O(100\ \text{m})$, was found numerically to satisfy $O(\tilde{k}\ \text{Re}) = 10^8$. This corresponds to $\nu = O(10^{-1})\ \text{m}^2\ \text{s}^{-1}$ if we take shear $S = 0.1$ and $\tilde{k} = 1$. This value of ν is larger than is realistic for diffusion in the troposphere. Furthermore, since the value of ν required to resolve the modes is proportional to the shear and wavenumber, the viscosity required becomes even less realistic as S and $\tilde{k}$ increase. Since the optimal evolution eventually converges to the most unstable mode (which in the presence of viscosity becomes the least damped mode), the optimal growth obtained in the viscid problem can be very different than that obtained in the inviscid problem for large times and large shears.

The viscid problem introduces an additional second derivative with height, which requires two additional boundary conditions. In order to prevent the boundaries from being a source of momentum, we require (in addition to the vanishing of the vertical velocity) the free-slip condition $\partial u/\partial z = \partial v/\partial z = 0$ at the boundaries. Similarly, to prevent the boundaries from being a thermal source, we set $\partial\theta/\partial z = 0$ there as well. In the QG limit, the momentum free-slip condition is equivalent to vanishing θ_y due to the thermal wind balance, and this boundary condition is in agreement with Bretherton's (1966) alternative description of the Eady basic state, which requires the zonal mean flow to satisfy $\overline{U}_z = -\overline{\theta}_y = 0$ on the boundaries. Since everywhere else within the domain the mean shear is a nonzero constant, in the limit, these boundary conditions form delta functions in $\overline{U}_{zz}$ with opposite signs just above the lower boundary and just below the upper boundary.

Here, $\overline{U}_{zz} = -\overline{q}_y$ where $\overline{q}_y$ is the mean PV gradient. Solving the QG PV equation, with this basic state and boundary conditions $\theta(z = 0; 1) = 0$, is equivalent to solving the PV equation within the domain and the thermodynamic equations on the boundaries in the conventional Eady model. Although we solve the PE, we would like to obtain the QG limit for large Richardson numbers and thus we adopt Bretherton's description and solve (A2) under the approximation to Bretherton's basic state:

$$\overline{U} = \begin{cases} \dfrac{1}{2}\left[\left(\dfrac{z^2}{z_B}\right) + z_B\right] \\ z \\ \dfrac{1}{2}\left[\dfrac{(1-z)^2}{(1-z_T) + (z_T+1)}\right]; \end{cases} \qquad \overline{U}_z = \begin{cases} \dfrac{z}{z_B} \\ 1 \\ \dfrac{(1-z)}{(1-z_T)}; \end{cases} \qquad \overline{U}_{zz} = \begin{cases} \dfrac{1}{z_B} & \text{for } 0 \le z < z_B \\ 0 & \text{for } z_B < z < z_T \\ -\dfrac{1}{(1-z_T)} & \text{for } z_T < z \le 1. \end{cases} \tag{B2}$$

As the numbers of layers increase, z_B and $(1 - z_T)$ can be taken to be smaller and in the continuous limit U_{zz} forms the boundary delta functions with opposite signs. When viscosity is small, the phase speeds, growth rates, and structures of the analytic PE normal modes that are obtained from using this basic state approximate the analytic PE normal modes obtained using the inviscid Eady model.

REFERENCES

Áranson, G., 1963: The stability of nongeostrophic perturbations in a baroclinic zonal flow. *Tellus,* **15,** 205–211.

Bannon, P. R., 1989: Linear baroclinic instability with the geostrophic momentum approximation. *J. Atmos. Sci.,* **46,** 402–409.

Blumen, W., 1975: An analytical view of updating meteorological variables: Part I. Phase errors. *J. Atmos. Sci.,* **32,** 274–286.

Bretherton, F. P., 1966: Baroclinic instability and the short wave cutoff in terms of potential vorticity. *Quart. J. Roy. Meteor. Soc.,* **92,** 335–345.

Derome, J., and C. L. Dolph, 1970: Three-dimensional non-geostrophic disturbances in a baroclinic zonal flow. *Geophys. Fluid Dyn.,* **1,** 91–122.

Dewar, W. K., and P. D. Killworth, 1995: Do fast gravity waves interact with geostrophic motions? *Deep-Sea Res.,* **42A,** 1063–1081.

Drazin, P. G., and W. H. Reid, 1981: *Hydrodynamic Stability.* Cambridge University Press, 525 pp.

Eady, E. T., 1949: Long waves and cyclone waves. *Tellus,* **1,** 33–52.

Farrell, B. F., 1984: Modal and non-modal baroclinic waves. *J. Atmos. Sci.,* **41,** 668–673.

——, and P. J. Ioannou, 1995: Stochastic dynamics of the midlatitude atmospheric jet. *J. Atmos. Sci.,* **52,** 1642–1656.

——, and ——, 1996: Generalized stability theory. Part I: Autonomous operators. *J. Atmos. Sci.,* **53,** 2025–2040.

Gill, A. E., 1982: *Atmosphere–Ocean Dynamics.* Academic Press, 662 pp.

Hoskins, B. J., I. Darghici, and H. C. Davies, 1978: A new look at the ω-equation. *Quart. J. Roy. Meteor. Soc.,* **104,** 31–38.

Koshyk, J. N., K. Hamilton, and J. D. Mahlman, 1999: Simulation of the $k^{-5/3}$ mesoscale spectral regime in the GFDL SKYHI general circulation model. *Geophys. Res. Lett.,* **26,** 843–846.

Mankin, M., 1977: On the nongeostrophic baroclinic instability problem. *J. Atmos. Sci.,* **34,** 991–1002.

Muraki, D. J., C. Snyders, and R. Rotunno, 1999: The next-order corrections to quasigeostrophic theory. *J. Atmos. Sci.,* **56,** 1547–1560.

Nakamura, N., 1988: Scale selection of baroclinic instability—Effects of stratification and nongeostrophy. *J. Atmos. Sci.,* **45,** 3253–3267.

Noble, B., and J. Daniel, 1988: *Applied Linear Algebra.* Prentice Hall, 521 pp.

Peixoto, J. P., and A. H. Oort, 1992: *Physics of Climate.* American Institute of Physics, 520 pp.

Snyder, C., 1995: Stability of steady fronts with uniform potential vorticity. *J. Atmos. Sci.*, **52,** 724–736.
Stone, P. H., 1966: On non-geostrophic baroclinic stability *J. Atmos. Sci.*, **23,** 390–400.
Warn, T., and R. Menard, 1986: Nonlinear balance and gravity–inertial wave saturation in a simple atmospheric model. *Tellus,* **38A,** 285–294.
Yamazaki, H. Y., and W. R. Peltier, 2001: On the existence of subsynoptic-scale baroclinic instability and the nonlinear evolution of shallow disturbances *J. Atmos. Sci.*, **58,** 657–683.